Volume 9
Number 7
21 February 2021
Pages 2207–2584

Journal of Materials Chemistry C

Materials for optical, magnetic and electronic devices

rsc.li/materials-c

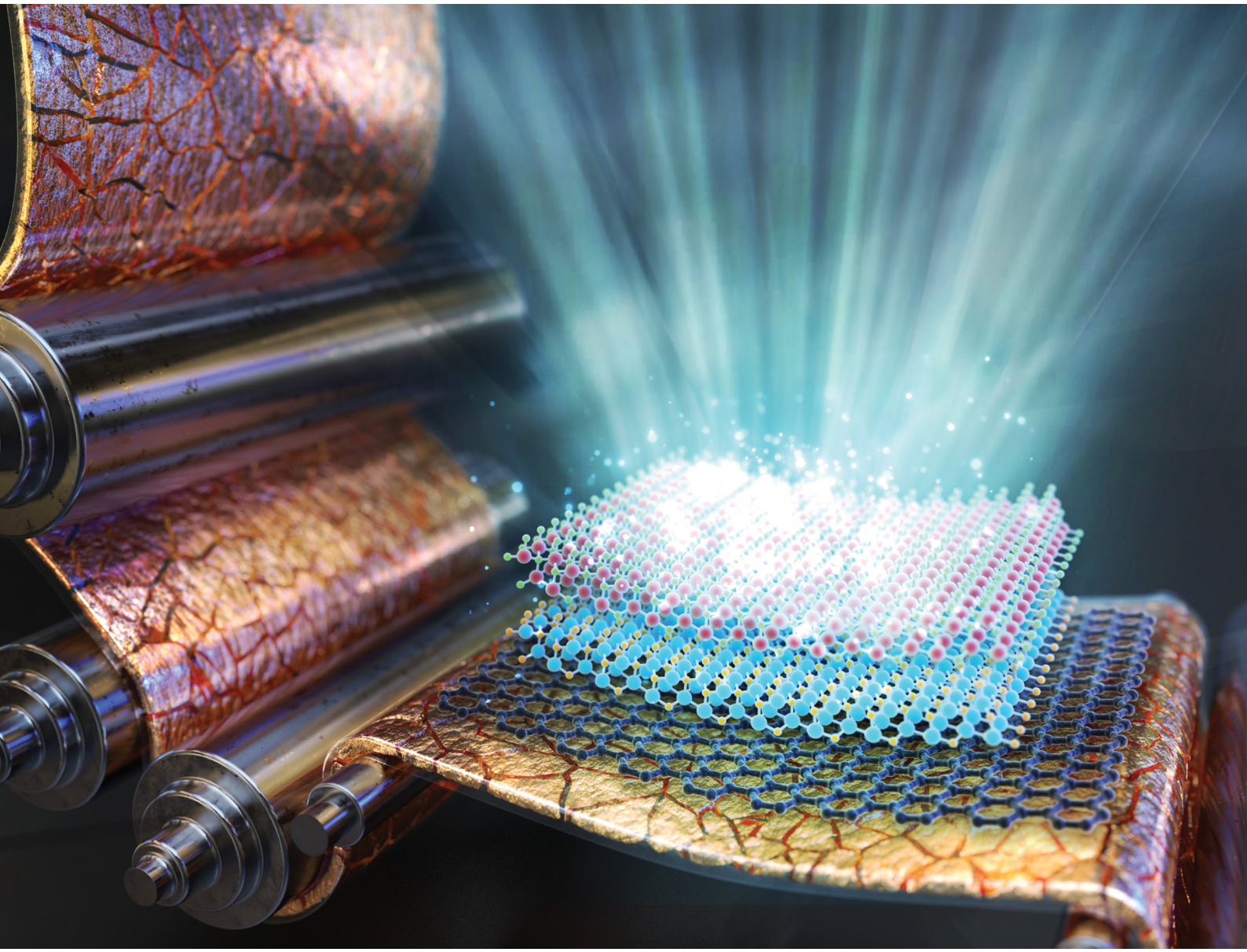

ISSN 2050-7526

ROYAL SOCIETY OF CHEMISTRY

PAPER

Jae-Hyun Ryou *et al.*

Flexible single-crystalline GaN substrate by direct deposition of III-N thin films on polycrystalline metal tape

Journal of Materials Chemistry C

ROYAL SOCIETY OF CHEMISTRY

PAPER

View Article Online
View Journal | View Issue

Cite this: J. Mater. Chem. C, 2021, 9, 2243

Flexible single-crystalline GaN substrate by direct deposition of III-N thin films on polycrystalline metal tape†

Shahab Shervin,‡[abc] Mina Moradnia,‡[ac] Md Kamrul Alam,[d] Tain Tong,[d] Mi-Hee Ji,[e] Jie Chen,[abc] Sara Pouladi,[bc] Theeradetch Detchprohm,[e] Rebecca Forrest,[f] Jiming Bao,[d] Russell D. Dupuis[e] and Jae-Hyun Ryou *[abc]

Flexible electronics and mechanically bendable devices based on Group III-N semiconductor materials are emerging; however, there are several challenges in manufacturing, such as cost reduction, device stability and flexibility, and device-performance improvement. To overcome these limitations, it is necessary to replace the brittle and expensive semiconductor wafers with single-crystalline flexible templates for a new-bandgap semiconductor platform. The substrates in the new concept of semiconductor materials have a hybrid structure consisting of a single-crystalline III-N thin film on a flexible metal tape substrate which provides a convenient and scalable roll-to-roll deposition process. We present a detailed study of a unique and simple direct epitaxial growth technique for crystallinity transformation to deliver single-crystalline GaN thin film with highly oriented grains along both *a*-axis and *c*-axis directions on a flexible and polycrystalline copper tape. A 2-dimensional (2D) graphene having the same atomic configuration as the (0001) basal plane of wurtzite structure is employed as a seed layer which plays a key role in following the III-N epitaxy growth. The DC reactive magnetron sputtering method is then applied to deposit an AlN layer under optimized conditions to achieve preferred-orientation growth. Finally, single-crystalline GaN layers (~1 μm) are epitaxially grown using metal organic chemical vapor deposition (MOCVD) on the biaxially-textured buffer layer. The flexible single-crystalline GaN film obtained using this method provides a new way for a wide-bandgap semiconductor platform pursuing flexible, high-performance, and versatile device technology.

Received 29th September 2020,
Accepted 28th December 2020

DOI: 10.1039/d0tc04634e

rsc.li/materials-c

Introduction

The group III-nitride (III-N) wide-bandgap (WBG) semiconductor has become a major material platform in solid-state electronics and photonics due to its excellent properties including a wide range of direct bandgap energies (E_g = 0.7–6.2 eV), high saturation velocity of carriers (~1.5–2 × 10^7 cm s^{-1}), and high breakdown field (~3–6 × 10^6 V cm^{-1}). Devices fabricated from the group III-nitride materials, therefore, play a dominant role in short-wavelength optoelectronics and high-frequency and high-power electronics.[1–5] III-N thin-film materials can be conventionally grown on single-crystalline sapphire (Al_2O_3), silicon carbide (SiC), and silicon (Si) (111) substrates by strained heteroepitaxy.[6] Sapphire is the most dominantly used substrate due to its relatively small thermal expansion coefficient (TEC) difference and in-plane lattice mismatch (LM) to achieve high-quality gallium nitride (GaN) and aluminum nitride (AlN) templates.[7,8] In-plane LMs and TEC differences between GaN and different substrates are shown in Fig. S1 (ESI†). Despite the small LM and TEC difference between SiC and GaN for high-quality epitaxial films, the wide adoption of SiC substrate in the commercial market has been hampered due to its high cost.[9] The use of Si (111) substrate generally results in an epitaxial film with a higher density of crystalline defects, even though this is the most economical approach for the manufacturing of III-N devices.[10,11]

[a] Department of Mechanical Engineering, University of Houston, Houston, Texas 77204-4006, USA. E-mail: jryou@uh.edu
[b] Materials Science and Engineering Program, University of Houston, Houston, Texas 77204, USA
[c] Texas Center for Superconductivity at UH (TcSUH) and Advanced Manufacturing Institute (AMI), University of Houston, Houston, Texas, 77204, USA
[d] Department of Electrical and Computer Engineering, University of Houston, Houston, Texas 77204, USA
[e] Center for Compound Semiconductors, School of Electrical and Computer Engineering, Georgia Institute of Technology, Atlanta, Georgia 30332-0250, USA
[f] Department of Physics, University of Houston, Houston, Texas 77204, USA

† Electronic supplementary information (ESI) available: TEC and LM calculation, AlN sputtering condition optimization, schematic of biaxial and uniaxial AlN growth, EBSD texture, and TEM analysis of GaN. See DOI: 10.1039/d0tc04634e

‡ These authors contributed equally to this work.

Demands for wearable and flexible devices are growing in solid-state lighting (SSL) and electronics for a wide range of applications such as bendable/curved luminaire and display of flexible electronics. Recent developments in flexible electronics demonstrate that semiconductor materials can be very flexible when their thickness is small enough (in the order of micrometers), deviating from the brittle nature of bulk properties.[12–16] However, currently developed substrates cannot provide a platform for flexible electronic and photonic devices due to the brittle nature of single-crystalline wafers with a thickness of hundreds of micrometers. Therefore, to fabricate mechanically flexible III-N devices and components, it is required to transfer the thin film for a device to a bendable secondary substrate followed by the removal of the original wafer substrate. This film-transfer technique involves additional complicated processing steps, hence it poses technical and economic challenges in the manufacturing of flexible semiconductor devices and systems, such as lower production yields, potential degradation of device performance, higher manufacturing cost, and process scalability limited by the current choices of wafer substrates. The challenges are associated with the current ''top-down'' process and can be resolved by adopting the ''bottom-up'' process. For the bottom-up process, it is necessary to begin with a flexible substrate instead of the brittle wafer substrates for the deposition of active thin-film device layers. However, all the current flexible substrates are non-single-crystalline materials. The deposition of thin films on such substrates results in non-single-crystalline materials for active semiconductor layers, which significantly degrade the performance characteristics of the devices. Therefore, to develop high-performance flexible devices, it is critical to obtain single-crystalline thin films even on non-crystalline substrates, overcoming the traditional epitaxial relationship between the substrate and the film.

In the present study, we develop a direct deposition technique in which III-N thin films of high crystalline quality can be epitaxially grown on a non-single-crystalline substrate. We demonstrate a single-crystalline GaN template layer on a flexible copper (Cu) tape substrate by employing graphene as the seed layer and AlN as the buffer layer. Direct growth of the 2D material on the polycrystalline substrate followed by the deposition of the buffer layer with crystallographically-selected orientations in both the in-plane and out-of-plane directions of the hexagonal lattice provides a critical solution for the crystallinity transformation from the polycrystalline substrate to single-crystalline GaN thin film. The result is a flexible single-crystalline GaN substrate consisting of a GaN template layer, crystallinity-transformational layers, and a Cu tape. The use of this new flexible, inexpensive, and lengthy tape substrate, instead of the brittle, expensive, and limited-area wafer substrates, will enable low-cost easily-scalable manufacturing of flexible wide-bandgap semiconductor devices compatible with the roll-to-roll process. Moreover, the flexible GaN substrate will help the easy fabrication of multifunctional III-N devices for electronic, photonic, sensing, and energy harvesting applications.[17–24] Among the potential applications, large-scale, flexible inorganic LEDs could be applied for flexible LED TV displays, large-scale energy-efficient lighting, or window displays in the future. Furthermore, single-crystalline, GaN-based, flexible electronics, which promise higher efficiency, reliability, and a longer lifetime, can replace organic flexible electronics in a range of applications, *i.e.*, biomedical applications exploiting high electron mobility transistor-based sensors or wearable electronics.

Experimental

Graphene growth on Cu

Chemical vapor deposition (CVD) was applied for the growth of graphene in a custom-built system, which consists of a quartz tube as the reaction chamber and a heating furnace with ~30 cm uniform temperature zone. Cu foil tapes with a thickness of 25 μm and a surface area of 16 × 21 mm^2 (99.8%, Alfa), sitting inside a quartz sample holder, were loaded into the reaction chamber and placed in the uniform-temperature zone of the furnace. The reaction chamber was evacuated thoroughly and then quickly filled to ambient pressure with argon (Ar) gas. Subsequently, the Cu tapes were annealed at 1050 °C in a slightly reducing environment using a mixture of Ar (600 sccm [standard cubic centimeters per minute]) and hydrogen (H_2, 60 sccm) during the heating and stabilizing process. A precursor with a mixture of methane (CH_4, 100 sccm) and H_2 (30 sccm) was introduced into the reaction chamber using Ar as the carrier gas (1200 sccm) for graphene growth for ~2 hours. Samples were fast-cooled down to room temperature after the shutoff of CH_4, typically within an hour, by pushing the sample holder out of the heating zone, under the protection of Ar and H_2.

AlN thin-film growth on graphene/Cu

AlN thin films were grown on the graphene-deposited Cu tapes using a DC reactive magnetron sputtering system (AJA International) equipped with a DC power supply (Advanced Energy MDX 500). The base and working pressures of the sputtering chamber were 10^{-9} Torr and 2 mTorr, respectively. The working pressure was set by adjusting a gate valve of a cryopump. The AlN films were deposited with an Al target (1.5 inch diameter, 99.5%, AJA International) at 110 W of a DC cathode power in a mixture of Ar and nitrogen (N_2) gases, which were introduced into the chamber by separate mass flow controllers. Before and during sputtering, the sample holder was rotated at 20 revolutions per minute (rpm) to ensure the uniformity of the film. Prior to each run, pre-sputtering was performed with Ar^+ ion bombardment to clean the Al target for 5 minutes with a movable shutter covering the substrate. Reactive sputtering was initiated by introducing N_2 into the chamber and opening the shutter. After the deposition, post-sputtering was performed for 10 min to avoid target poisoning. The oxygen (O_2) and water (H_2O) partial pressures in the chamber were monitored using a residual gas analyzer (RGA) (Kurt J. Lesker) and kept as low as 10^{-10} Torr and 10^{-11} Torr, respectively. A 200 nm-thick AlN film was deposited for 90 minutes under optimized conditions.

GaN thin-film growth on AlN/graphene/Cu

Epitaxial GaN layers were grown using a metal organic chemical vapor deposition (MOCVD) method in a 6 × 2″ reactor system

equipped with a close-coupled showerhead chamber (Thomas Swan). Trimethylgallium (TMGa, $Ga(CH_3)_3$), and ammonia (NH_3) were used as Group-III and Group-V precursors with H_2 carrier gas. The growth of the GaN layer was carried out at a chamber pressure of 500 Torr and a temperature of 900–950 °C for a target thickness of ~1 μm. The growth temperature was intentionally set at lower than the typical growth temperature of GaN by MOCVD (~1050 °C) due to a concern of potential damage to the Cu tape by overshooting during heating-up.

Characterization studies

The graphene was characterized using Raman spectroscopy using a 532 nm solid-state laser as the source of excitation in a home-built setup with a spectrometer (Horiba Jobin Yvon) at room temperature. Microscopic surface morphology of the graphene and III-N layers was characterized using atomic force microscopy (AFM) (Veeco Dimensions 3000). Microscopic surface images were taken using scanning-electron microscopy (SEM) (JEOL JSM 6400). Structural and crystalline qualities of the AlN and GaN layers were characterized using electron backscattered diffraction (EBSD) (Hikari Super EBSD camera from Ametek/EDAX attached to a Philips XL 30SFEG electron microscope) and high-resolution X-ray diffraction (HR-XRD) (Bruker D8 with the parallel beam for thin-film characterization).

Results

2-Dimensional material seed layer

A planar hexagonal atomic configuration of sp^2 bonded carbon atoms in graphene, which also creates weak van der Waals out-of-plane bonding at the cleavage planes, is expected to provide the preferential nucleation sites for the epitaxial growth of the hexagonal-lattice 3-dimensional structures. A graphene domain can grow over polycrystalline Cu grains crossing the grain boundaries of Cu due to the weak interaction between them for the surface catalyzed process; hence, there is no epitaxial relationship between the Cu lattice and graphene grains.[25] Therefore, a relatively large single-crystalline graphene grain can be formed on polycrystalline Cu foil.[25] Fig. 1a shows the microscopic surface image of a graphene film on a Cu tape substrate grown using the chemical vapor deposition (CVD) method. The presence of wrinkles (indicated using yellow arrows in the scanning-electron microscopy (SEM) image shown in Fig. 1a) confirms that the graphene film is continuous. The wrinkles are formed as the graphene expands during cool-down due to its negative TEC value. The red arrow shows a grain boundary of Cu, which also indicates that the graphene domain covers the multiple grains of the Cu. The average grain size of Cu is estimated to be ~0.5 mm. The Raman spectrum of the graphene shown in Fig. 1b presents a typical feature of few-layered graphene with a symmetric 2D-band peak centered at about 2690 cm^{-1} with a full-width-at-half-maximum (FWHM) of ~40 cm^{-1}. The intensity ratio of the 2D-band peak to G-band peak (I_{2D}/I_G) is sensitive to the layer numbers of graphene and characterizes the disorder degree of graphene.[26,27] I_{2D}/I_G is found to be ~1.6 and no D-band peak is present, confirming that high-quality defect-free graphene with less than three layers is grown on the Cu tape substrate.

AlN buffer layer

A suitable choice of a buffer layer between the substrate and epitaxial film is critical to improve the crystalline quality of the III-N films grown by strained heteroepitaxy.[28–31] Especially, the growth of a GaN layer, which serves as a template for most III-N devices, on the graphene is significantly different from those on other bulk substrates. For the epitaxial growth of 3D materials on 2D substrates, it is necessary to have at least one side of the interface with dangling bonds. However, the lack of dangling bonds in graphene, which makes it chemically inert with a very low surface energy, causes a thermodynamic problem for the

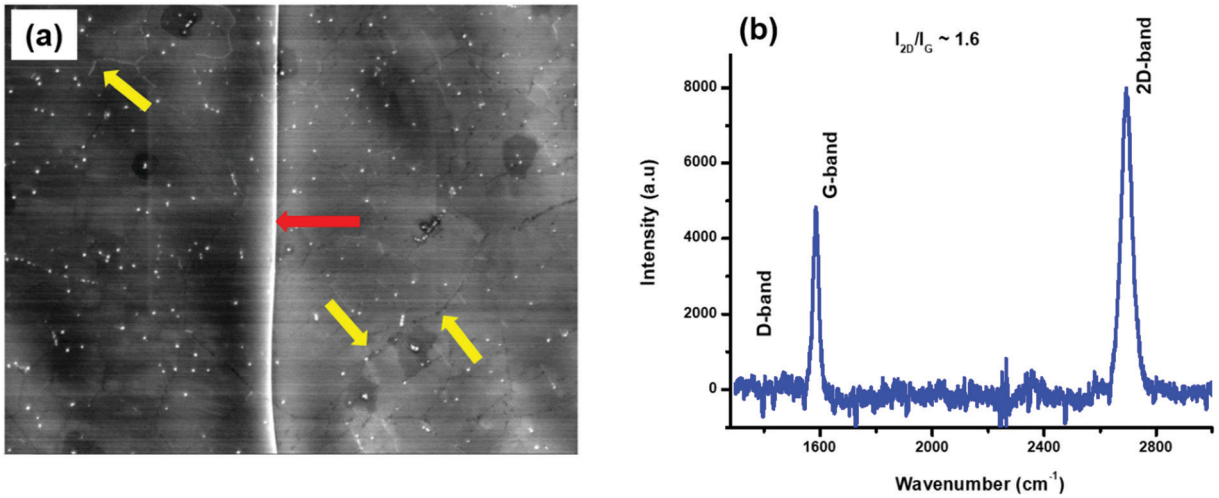

Fig. 1 (a) SEM image and (b) Raman spectrum of a graphene film on a Cu tape substrate grown using CVD. In (a) the red arrow points to a grain boundary of Cu and yellow arrows point to graphene wrinkles. In (b) the intensity ratio of the 2D-band peak to G-band peak (I_{2D}/I_G) is ~1.6 and no D-band peak is present, confirming that high-quality defect-free graphene with less than three layers is formed.

nucleation of foreign atoms with the strong sp^3 bonding of GaN.[32] Therefore, directly-grown GaN thin films on graphene were found to contain microstructural defects.[32–34] For the epitaxial growth of GaN on graphene, it is necessary to mitigate the large surface free energy difference between GaN and graphene layers (1970 and 52 mJ m^{-2}, respectively) by introducing an appropriate nucleation layer compensating the lack of dangling bonds on the graphene surface.

We employed an AlN buffer by sputtering, which has reasonable dangling bonds and comparable surface energy to promote uniform nucleation of the III-N layers. The AlN possesses the same crystal structure as GaN and its basal plane has the same atomic configuration to the underlying 2D material.[33,35] The sputtered AlN film does not necessarily follow the crystal structure of the underlying layer and sputtering parameters directly affect the final structure and quality of the deposited thin film. Reactive sputtering parameters of the AlN film, such as deposition rate, the target-to-substrate distance, and a ratio of reactive ion gas flow rate to total flow rate, were optimized based on the X-ray diffraction (XRD) characterization results. The Si (100) substrate was used for the calibration of AlN sputtering parameters due to its easy availability. On introducing N_2 gas to the Ar plasma, the deposition rate decreases drastically, as the collision of particles in the plasma increases. A reactive gas ratio was optimized at $R = \sim 44\%$ with flow rates of Ar and N_2 set at 10 sccm and 8 sccm, respectively, based on the XRD 2theta–omega (2θ–ω) scans (Fig. S2 (ESI†)) to achieve the highly *c*-axis-textured AlN in the out-of-plane direction. The mean free path (λ) of sputtered atoms should be larger than the target-to-substrate distance (d). The mean free path of Al atoms, which depends on the working pressure, $\lambda = \sim 10$ cm at $P = 2$ mTorr;[36,37] hence, the substrate should be kept less than 10 cm away from the target. The optimum target-to-substrate distance of $d = 8$ cm was obtained using a reactive gas ratio of $R = \sim 44\%$ (Fig. S3 (ESI†)).

Fig. 2a shows the XRD 2θ–ω scans of the AlN films on the graphene/Cu substrates at various deposition temperatures. For all the deposition temperatures, the AlN films are preferably grown in the *c*-axis of wurtzite structure normal to the surface, *i.e.*, along the out-of-plane direction. However, small peaks of $(10\bar{1}0)$ and $(10\bar{1}1)$ are also detected for AlN deposited at lower temperatures (400–600 °C), showing the minor polycrystalline nature of the AlN films, which may originate from adatoms' energy reaching the substrate and bombardment of sputtering ions.[38] Fig. 2b compares the FWHM values of the peaks from AlN (0002) rocking curves (ω scan) at various deposition temperatures. With increasing deposition temperature, the FWHM values decrease, indicating less spread in the tilt of the *c*-plane out of surface; hence, the crystalline quality of the AlN film is improved. The alignment of the *c*-axis of AlN in the out-of-plane direction is confirmed (refer to the uniaxially textured structure schematically shown in Fig. S4a (ESI†)).

To achieve the single-crystallinity of the film, the in-plane alignment (*a*-axis) as well as out-of-plane alignment of AlN needs to be confirmed. To evaluate the in-plane alignment of the deposited AlN films, an XRD phi (φ) scan was performed by rotating the sample at the diffraction angles of AlN $\{10\bar{1}2\}$ asymmetric planes, *i.e.*, $\omega = 42.73°$ and $2\theta = 49.84°$. Fig. 3a shows the XRD φ scan for the peaks of $\{10\bar{1}2\}$ planes of the AlN film deposited at 650 °C. Six peaks separated by 60°, showing the six-fold rotational symmetry, are observed, which confirms that the AlN film is highly aligned in both *a*-axis and *c*-axis directions (refer to the biaxially textured structure schematically shown in Fig. S4b (ESI†)). The FWHM value for one of the peaks is estimated to be $\Delta\varphi_{\mathrm{AlN}\,(10\bar{1}2)} = \sim 4°$. The electron backscatter diffraction (EBSD) data further confirm the single-crystalline nature of AlN. Fig. 3b shows that the surface of the AlN has a uniform (0001) plane. The pole figures shown in Fig. 3c also indicate intense (0001) reflections at the center, showing the growth of highly *c*-axis oriented AlN. Furthermore, a clear six-fold rotational symmetric feature is observed in the pole figures of $(11\bar{2}0)$ and $(10\bar{1}0)$ planes. Fig. 3d and e show the crack-free and flat surface morphology of the AlN.

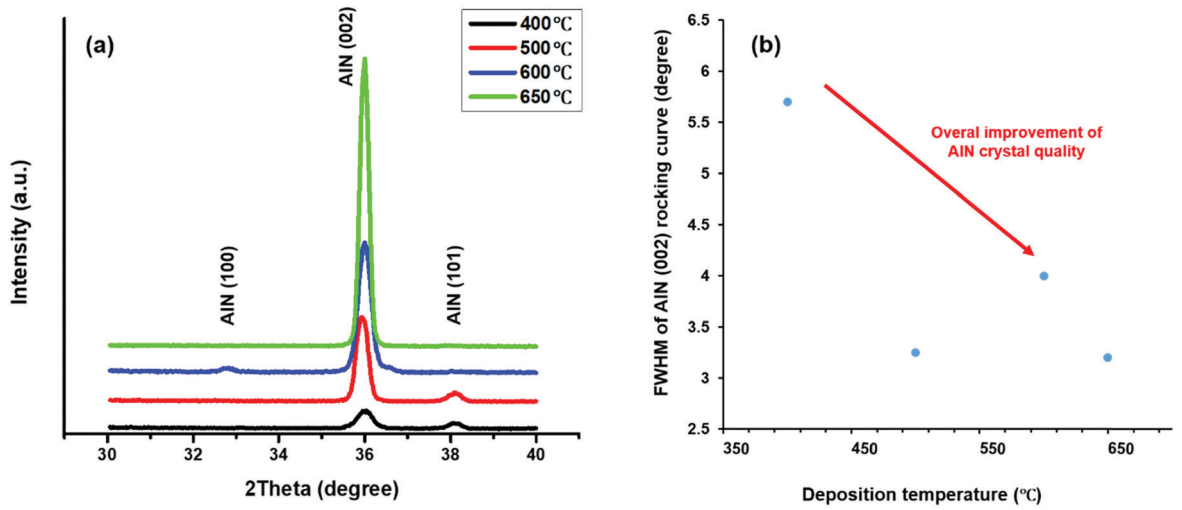

Fig. 2 (a) XRD 2θ-ω scans and (b) FWHM values of the AlN (0002) peak measured using XRD rocking curves (ω scans) for AlN layers on graphene/Cu tape substrates deposited at different temperatures.

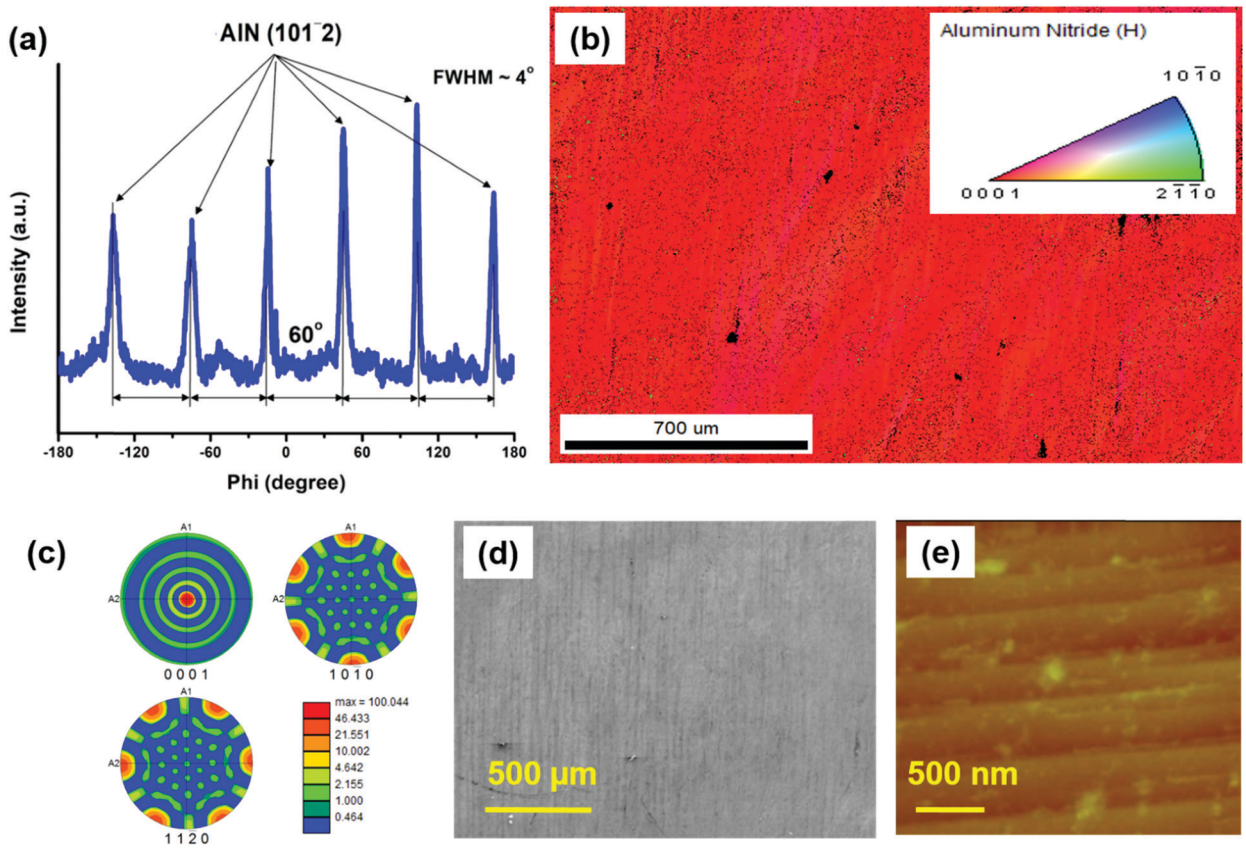

Fig. 3 (a) XRD φ scan of AlN {10$\bar{1}$2} peaks, (b) color-coded orientation map and (c) (0001), (10$\bar{1}$0), and (11$\bar{2}$0) pole figures measured using EBSD, (d) SEM and (e) AFM (2.5 × 2.5 μm^2 with z scale of 65 nm) images of an AlN film on a graphene/Cu tape substrate.

The root-mean-square (rms) roughness of the AlN surface measured using AFM is ~6 nm.

GaN template layer

After the successful development of nearly a single-crystalline AlN buffer layer, the epitaxial growth of a GaN film becomes less challenging. Fig. 4a shows an XRD 2θ–ω scan in a wide range for the GaN directly grown on the AlN/graphene/Cu substrate. The presence of only (000l) peaks such as (0002) and (0004) peaks and no other peak of GaN and AlN further confirm the epitaxial growth of III-N films along the c-axis of the wurtzite structure on graphene. The polycrystalline nature of the Cu tape is clear from different peaks related to different crystallographic orientations of the Cu grains. Fig. 4b shows the XRD φ (rotational) scan around GaN {10$\bar{1}$2}. Again, six separate peaks 60° apart indicate both the in-plane and out-of-plane alignments, supporting the epitaxial growth of a single-crystalline GaN film. The XRD results also show that the crystalline quality of GaN is further improved. The FWHM values of the peaks are slightly decreased compared to those of AlN peaks, $\Delta\varphi_{\mathrm{GaN}\ (10\bar{1}2)} < \sim 3^\circ$. Considering the large size of the XRD slit and the low $\Delta\varphi$ values in the GaN {10$\bar{1}$2} peaks, it is clear that single-crystalline GaN domains are large enough in the range of more than hundreds of micrometers and millimeters.

Motivated by scientific interests and practical importance, the epitaxial growth of the III-N films on graphene has been actively investigated using different approaches in recent years. Among them, Yu *et al.* reported a direct growth of GaN on flexible graphene-deposited Cu substrates. While the single-crystalline AlN and GaN were claimed under selected conditions, it was not fully confirmed using characterization studies in a large area such as an asymmetric XRD scan.[39] Moreover, the study employed migration-enhanced molecular beam epitaxy (ME-MBE), which is an inherently very low throughput process. Another work by Ramesh *et al.* using laser molecular beam epitaxy (LMBE) for the growth of GaN film on graphene/Cu foil reported a non-single-crystalline mixed-phase of the GaN grain film.[40] Chung *et al.*'s work employed a high throughput CVD process to grow a GaN film on a non-single-crystalline silica substrate.[41] However, the work was not a direct growth process, as the graphene layer had to be transferred to a substrate. Also, the substrate was not mechanically flexible which makes the process incompatible to the roll-to-roll process and flexible devices. Kim *et al.* and Balushi *et al.* reported single-crystalline GaN and AlN layers on a graphene/(0001) SiC wafer substrate.[33,42] Also, Zhang *et al.* reported the reduced threading dislocation density in the GaN grown on graphene/AlN on a (0001) sapphire substrate.[43] In these studies, it is not clear if the epitaxial growth occurs on graphene, as the single-crystalline SiC (or AlN) can also play a role in the epitaxial growth. The studies also require an additional transfer process for flexible devices. Our study is the first to demonstrate the growth of single-crystalline GaN directly

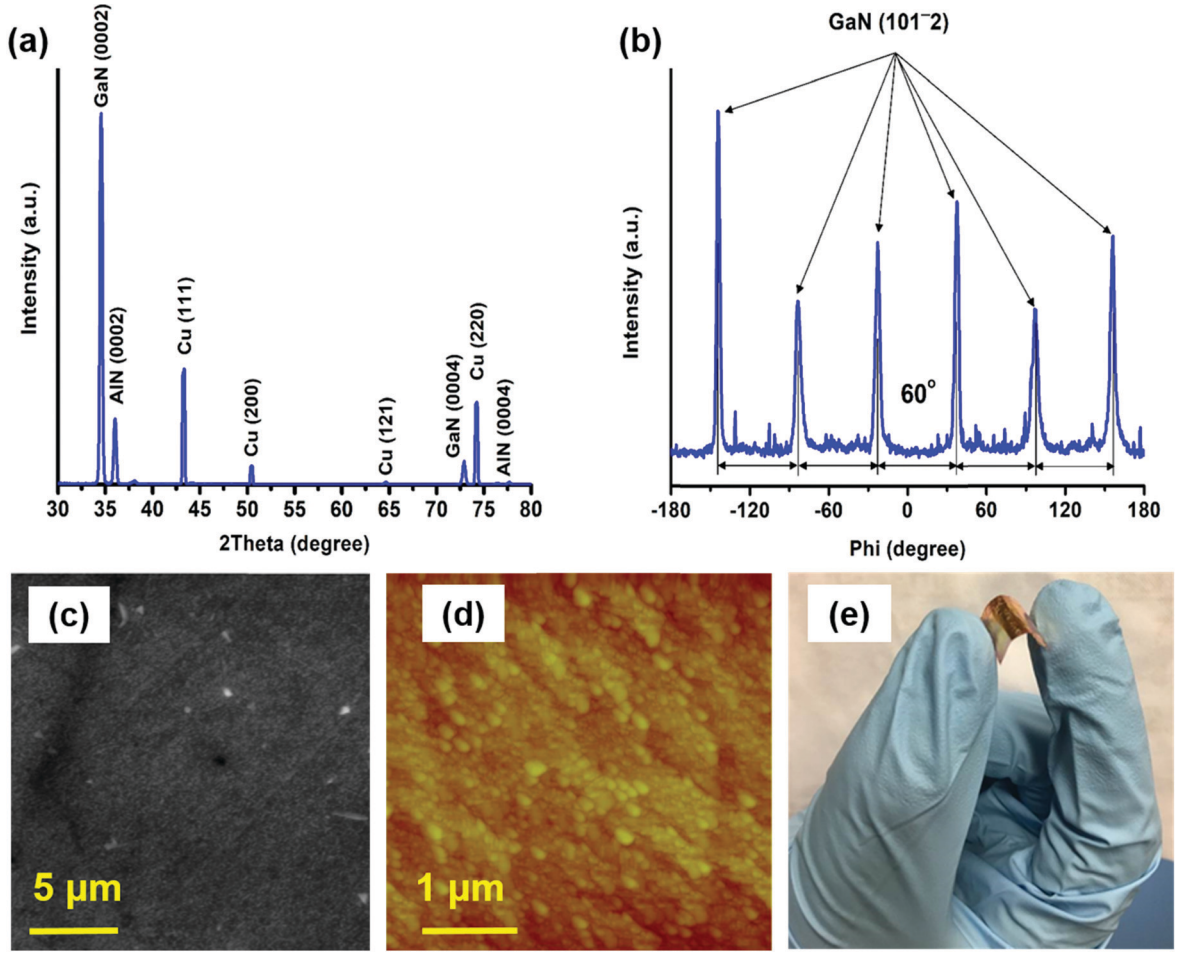

Fig. 4 (a) XRD 2θ-ω scan of GaN on AlN/graphene/Cu foil, (b) XRD φ scan of GaN $\{10\bar{1}2\}$ peaks, (c) SEM and (d) AFM (4×4 μm^2 with z scale of 80 nm) images for a GaN film on an AlN/graphene/Cu tape substrate. (e) Photo of a flexible GaN substrate consisting of a GaN template layer on Cu tape with graphene/AlN seed/buffer layers.

on polycrystalline flexible metal tape using high throughput processes.

The outcome of this single-crystalline GaN epitaxy produces a flexible GaN substrate consisting of a GaN template layer on a Cu tape with transfer-free seed/buffer layers as can be seen in the photo shown in Fig. 4e. The EBSD characterization further confirms the formation of a single-crystalline GaN film (Fig. S5a and b (ESI†)). However, the AlN and GaN films contain threading dislocations as shown in the cross-sectional transmission-electron microscopy (TEM) image in Fig. S5c (ESI†), similar to all the III-N epitaxial films grown by heteroepitaxy. The density of threading dislocations in the single-crystalline GaN layer is estimated to be $\sim 4 \times 10^{10}$ cm^{-2} and $\sim 7 \times 10^{10}$ cm^{-2} for screw and edge dislocations, respectively, from XRD rocking curves of (0002) and $(10\bar{1}2)$ planes using a method suggested by Kaganer *et al.*[44] The density is higher than the typical values of well-matured GaN epitaxial films on single-crystalline substrates of SiC, sapphire, and Si (*e.g.*, 10^8–10^9 cm^{-2}), as expected. The density of dislocation needs to be reduced by further optimization of the deposition processes to achieve devices with comparable performance to wafer-based non-flexible devices. Fig. 4c and d show the surface morphology of the GaN layer. The SEM image shows a continuous film with a similar surface to that of AlN. The surface of the GaN probed using AFM was found to be slightly rougher than that of AlN, possibly due to the lower growth temperature than the typical MOCVD growth temperatures of GaN by 100–150 °C.

van der Waals epitaxy *vs.* remote epitaxy

Single-crystalline AlN is confirmed to be epitaxially grown on the graphene layer. van der Waals epitaxy (vdWE) was proposed as a possible mechanism of the growth of a thin-film on a 2D material. The vdWE is different from the conventional epitaxy where strong chemical bonding exists at the interface of the substrate and epitaxial materials. The vdWE makes crystalline growth possible between 2D and 3D materials by weak van der Waals interaction at the heterojunction. The vdWE eliminates the necessity of reducing the lattice mismatch between epitaxial layers and underlying 2D materials and allows the heteroepitaxial growth for various materials with different crystal structures due to the absence of broken bonds on the vdW surface.[40,45] The vdWE has been experimentally observed in the III-N film on graphene.

Qi *et al.* introduced graphene as an interlayer for the growth of AlN on a sapphire substrate. Decreasing threading dislocations along with strain relaxation could come from reducing the lattice mismatch between AlN and the sapphire substrate by graphene.[46] Despite the less crystalline quality of GaN which was grown on the transferred multilayer graphene on sapphire, Li *et al.* found that light-emitting diodes grown on such multilayer graphene resulted in high output power.[47] These results could address the problem of large lattice and thermal mismatch between the III-N films and substrate by using multilayer graphene. However, in the previous reports, the growth of III-N occurred on the graphene that was transferred onto a sapphire substrate, *i.e.*, on a graphene/sapphire substrate. Therefore, the epitaxy of III-N film was not confirmed to originate from either graphene or sapphire. The epitaxial relationship between III-N and the sapphire substrate was reported, suggesting that the III-N epitaxy may have still originated from sapphire.[48] Kim *et al.* recently introduced remote epitaxy as another possible epitaxial growth mechanism of the thin film on 2D materials. The remote epitaxy occurs when the substrate directly affects the orientation of epitaxial growth and transfers its crystallographic information to the over-layers during the epitaxy. Because of the sufficiently thin and electrical penetration characteristics of graphene, the over-layers can follow the orientation of the underlying substrate.[49]

This study provides an ideal structure to study the mechanism of III-N epitaxy on graphene, which is still inconclusive because it uses a polycrystalline substrate underneath the graphene. In the III-N epitaxial layers on graphene/Cu of the present study, AlN and GaN are single-crystalline while Cu is polycrystalline as described earlier (Fig. 3a and 4a and b), which provides evidence to support vdWE over remote epitaxy. According to the remote epitaxy mechanism in which a structure mirroring of a substrate happens in an over-layer, the graphene interlayer should transfer the crystallographic structure of the underlying Cu substrate to the AlN over-layer. If the remote epitaxy is the dominant mechanism of the III-N epitaxy on a graphene/underlying substrate, III-N films tend to be polycrystalline too. The remote epitaxy mechanism cannot explain the single-crystal growth of III-N on the polycrystalline Cu substrate. A further comprehensive study was performed on the structural properties of AlN films deposited on different substrates of poly- and single-crystals in combination with/without the graphene layer, as shown in Fig. 5. All the AlN layers are uniaxially textured along the *c*-axis of the wurtzite structure regardless of the substrate when the optimized sputtering condition was employed (Fig. 5a). This is conventionally observed for AlN deposited by sputtering mainly due to the surface energy of its polar surface.[50] The crystalline quality of the films appears to be the best and worst for the AlN on graphene/single-crystalline Cu and polycrystalline Cu without graphene, respectively, from the intensity and FWHM of the AlN (0002) peaks (Fig. 5a). In-plane alignment, however, cannot be obtained without the help of epitaxial relationships from the underlying layer. Fig. 5b shows the XRD φ scan around AlN $\{10\bar{1}2\}$ planes. All the AlN films grown on graphene show the in-plane alignment of single-crystals regardless of the crystallinity of Cu, *i.e.*, on graphene/single-crystalline Cu (black curve of Fig. 5b) and graphene/polycrystalline Cu (red curve of Fig. 5b). In contrast, no in-plane alignment is observed for AlN on polycrystalline Cu without graphene (green curve of Fig. 5b). These results further support the vdWE for III-N on graphene. In other words, single-crystalline III-N can only be epitaxially grown on graphene. Only polycrystalline uniaxially textured AlN can be achieved without graphene, suggesting that AlN single-crystal growth cannot occur without the effect of graphene on the polycrystalline Cu while it is independent of copper crystal orientation.[51] To exclude the possibility of polycrystalline AlN growth by non-optimized deposition condition on Cu, we deposited AlN on a single-crystalline Cu

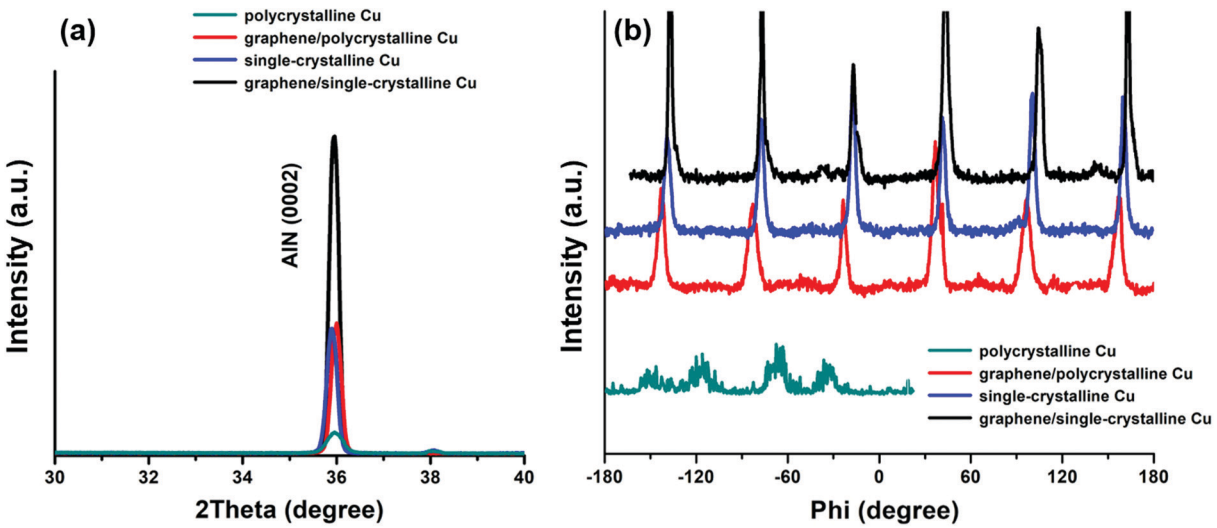

Fig. 5 (a) XRD 2θ-ω scans and (b) XRD φ scan of $\{10\bar{1}2\}$ peaks of an AlN layer on different substrates including single-crystalline Cu without graphene (blue curve), graphene/single-crystalline Cu (black curve), graphene/polycrystalline Cu (red curve), and polycrystalline Cu without graphene (green curve) substrates.

substrate without graphene under the same conditions. The AlN is single-crystalline on a single-crystalline Cu substrate without graphene (blue curve of Fig. 5b). Therefore, these results suggest that the epitaxy of III-N is influenced by the directly underlying layer and vdWE occurs for the growth of III-N layers on the graphene/Cu substrate.

GaN and Cu (111) have a significant discrepancy in LM and TEC. Graphene growth is of critical importance for reducing the effect of the lattice mismatch between AlN and copper foil, which comes from the vdWE growth for III-nitrides on graphene.[32,41] Thanks to the weak vdW bonding between AlN and graphene, AlN can be epitaxially grown on a Cu substrate without the necessity of reducing LM and TEC mismatch between AlN and Cu (111) substrate.

Conclusions

We developed a unique structure material, which enables continuous roll-to-roll (R2R) thin-film epitaxial GaN growth on low-cost and bendable Cu poly-crystalline tape, by employing suitable buffer layers. In this method, a 2D graphene interlayer grown using a CVD method provides an in-plane hexagonal atomic arrangement for single-crystalline AlN buffer layer growth by vdW epitaxy growth. Optimized conditions for DC reactive magnetron sputtering were applied to achieve the preferred-orientation AlN buffer. The XRD pole-figure of AlN ($10\bar{1}2$) shows a six-fold symmetry of AlN which is highly textured in both *a*-axis and *c*-axis crystallographic directions. The single-crystalline wurtzite structure of GaN is formed on the biaxial textured AlN buffer layer by MOCVD. The XRD 2θ–ω scan shows that the *c*-plane of GaN and AlN films is preferably grown from the (0002) and (0004) peaks. The outcome is the flexible single-crystalline GaN substrate on Cu tape. The present findings, focusing on the interface, epitaxial relationship, and vdW epitaxy growth mechanisms to achieve single-crystalline III-nitride materials on flexible/polycrystalline substrates, offer a promising solution to meet the rapidly increasing demand for bendable/curved luminaire and display of flexible electronics.

Conflicts of interest

There are no conflicts to declare.

Acknowledgements

The work at the University of Houston was partially supported by the National Science Foundation under Grant No. 1842299 (Electrical, Communications and Cyber Systems (ECCS)) and Grant No. 1907626 (I-CORPS of Industrial Innovation and Partnerships (IIP)) and King Abdullah University of Science and Technology (KAUST), Saudi Arabia (Contract No. OSR-2017-CRG6-3437.02). J. H. R. also acknowledges partial support from the Texas Center for Superconductivity at the University of Houston (TcSUH) and Advanced Manufacturing Institute (AMI).

References

1 M. R. Krames, O. B. Shchekin, R. Mueller-Mach, G. O. Mueller, L. Zhou, G. Harbers and M. G. Craford, *J. Disp. Technol.*, 2007, **3**, 160–175.
2 F. A. Ponce and D. P. Bour, *Nature*, 1997, **386**, 351–359.
3 S. T. Sheppard, K. Doverspike, W. L. Pribble, S. T. Allen, J. W. Palmour, L. T. Kehias and T. J. Jenkins, *IEEE Electron Device Lett.*, 1999, **20**, 161–163.
4 J. B. Limb, D. Yoo, J. H. Ryou, W. Lee, S. C. Shen, R. D. Dupuis, M. L. Reed, C. J. Collins, M. Wraback, D. Hanser, E. Preble, N. M. Williams and K. Evans, *Appl. Phys. Lett.*, 2006, **89**, 011112.
5 M. Ishida, T. Ueda, T. Tanaka and D. Ueda, *IEEE Trans. Electron Devices*, 2013, **60**, 3053–3059.
6 J.-H. Ryou, in *Nitride Semiconductor Light-Emitting Diodes (LEDs): Materials, Technologies, and Applications*, ed. J.-J. Huang, H.-C. Kuo and S.-C. Shen, Elsevier, Amsterdam, 2nd edn, 2017, vol. 3, pp. 66–98.
7 S. Nakamura, *Jpn. J. Appl. Phys.*, 1991, **30**, L1705–L1707.
8 H. Okano, N. Tanaka, Y. Takahashi, T. Tanaka, K. Shibata and S. Nakano, *Appl. Phys. Lett.*, 1994, **64**, 166–168.
9 M. A. L. Johnson, S. Fujita, W. H. Rowland, K. A. Bowers, W. C. Hughes, Y. W. He, N. A. El Masry, J. W. Cook, J. F. Schetzina, J. Ren and J. A. Edmond, *Solid-State Electron.*, 1997, **41**, 213–218.
10 H. Liu, Z. Ye, H. Zhang and B. Zhao, *Mater. Res. Bull.*, 2000, **35**, 1837–1842.
11 A. M. Mizerov, S. N. Timoshnev, M. S. Sobolev, E. V. Nikitina, K. Y. Shubina, T. N. Berezovskaia, I. V. Shtrom and A. D. Bouravleuv, *Semiconductors*, 2018, **52**, 1529–1533.
12 D. Shahrjerdi and S. W. Bedell, *Nano Lett.*, 2013, **13**, 315–320.
13 S. Pouladi, M. Rathi, D. Khatiwada, M. Asadirad, S. K. Oh, P. Dutta, Y. Yao, Y. Gao, S. Sun, Y. Li, S. Shervin, K. H. Lee, V. Selvamanickam and J. H. Ryou, *Prog. Photovoltaics*, 2019, **27**, 30–36.
14 M. Asadirad, Y. Gao, P. Dutta, S. Shervin, S. Sun, S. Ravipati, S. H. Kim, Y. Yao, K. H. Lee, A. P. Litvinchuk, V. Selvamanickam and J. H. Ryou, *Adv. Electron. Mater.*, 2016, **2**, 1600041.
15 W. Wang, J. Chen, J. S. Lundh, S. Shervin, S. K. Oh, S. Pouladi, Z. Rao, J. Y. Kim, M.-K. Kwon, X. Li, S. Choi and J.-H. Ryou, *Appl. Phys. Lett.*, 2020, **116**, 123501.
16 J. Chen, S. K. Oh, N. Nabulsi, H. Johnson, W. Wang and J. H. Ryou, *Nano Energy*, 2019, **57**, 670–679.
17 N. I. Kim, Y. L. Chang, J. Chen, T. Barbee, W. Wang, J. Y. Kim, M. K. Kwon, S. Shervin, M. Moradnia, S. Pouladi, D. Khatiwada, V. Selvamanickam and J. H. Ryou, *Sens. Actuators, A*, 2020, **305**, 111940.
18 J. Chen, H. Liu, W. Wang, N. Nabulsi, W. Zhao, J. Y. Kim, M. K. Kwon and J. H. Ryou, *Adv. Funct. Mater.*, 2019, **29**, 1903162.
19 J. Chen, S. K. Oh, H. Zou, S. Shervin, W. Wang, S. Pouladi, Y. Zi, Z. L. Wang and J. H. Ryou, *ACS Appl. Mater. Interfaces*, 2018, **10**, 12839–12846.
20 W. Wang, S. Shervin, S. Member, S. K. Oh, J. Chen, Y. Huai, S. Pouladi, H. Kim, S. Lee, J. Ryou and S. Member, *IEEE Electron Device Lett.*, 2017, **38**, 1086–1089.

21 S. Shervin, *et al.*, Flexible deep-ultraviolet light-emitting diodes for significant improvement of quantum efficiencies by external bending, *J. Phys. D: Appl. Phys.*, 2018, **51**, 105105.
22 S. Shervin, S. H. Kim, M. Asadirad, S. Y. Karpov, D. Zimina and J. H. Ryou, *ACS Photonics*, 2016, **3**, 486–493.
23 S. Shervin, S. H. Kim, M. Asadirad, S. Ravipati, K. H. Lee, K. Bulashevich and J. H. Ryou, *Appl. Phys. Lett.*, 2015, **107**, 193504.
24 N. Palavesam, S. Marin, D. Hemmetzberger, C. Landesberger, K. Bock and C. Kutter, *Flexible Printed Electron.*, 2008, **3**, 014002.
25 Q. Yu, L. A. Jauregui, W. Wu, R. Colby, J. Tian, Z. Su, H. Cao, Z. Liu, D. Pandey, D. Wei, T. F. Chung, P. Peng, N. P. Guisinger, E. A. Stach, J. Bao, S. S. Pei and Y. P. Chen, *Nat. Mater.*, 2011, **10**, 443–449.
26 X. Li, W. Cai, J. An, S. Kim, J. Nah, D. Yang, R. Piner, A. Velamakanni, I. Jung, E. Tutuc, S. K. Banerjee, L. Colombo and R. S. Ruoff, *Science*, 2009, **324**, 1312–1314.
27 L. M. Malard, M. A. Pimenta, G. Dresselhaus and M. S. Dresselhaus, *Phys. Rep.*, 2009, **473**, 51–87.
28 T. Warren Weeks, M. D. Bremser, K. S. Ailey, E. Carlson, W. G. Perry and R. F. Davis, *Appl. Phys. Lett.*, 1995, **67**, 401–403.
29 E. Feltin, B. Beaumont, M. Laügt, P. De Mierry, P. Vennéguès, H. Lahrèche, M. Leroux and P. Gibart, *Appl. Phys. Lett.*, 2001, **79**, 3230–3232.
30 H. Amano, N. Sawaki, I. Akasaki and Y. Toyoda, *Appl. Phys. Lett.*, 1986, **48**, 353–355.
31 W. H. Sun, J. P. Zhang, J. W. Yang, H. P. Maruska, M. A. Khan, R. Liu and F. A. Ponce, *Appl. Phys. Lett.*, 2005, **87**, 211915.
32 J. H. Choi, J. Kim, H. Yoo, J. Liu, S. Kim, C. W. Baik, C. R. Cho, J. G. Kang, M. Kim, P. V. Braun, S. Hwang and T. S. Jung, *Adv. Opt. Mater.*, 2016, **4**, 505–521.
33 Z. Y. Al Balushi, T. Miyagi, Y. C. Lin, K. Wang, L. Calderin, G. Bhimanapati, J. M. Redwing and J. A. Robinson, *Surf. Sci.*, 2015, **634**, 81–88.
34 A. Ishii, T. Tatani, H. Asano and K. Nakada, *Phys. Status Solidi C*, 2010, **7**, 347–350.
35 Q. Zeng, Z. Chen, Y. Zhao, T. Wei, X. Chen, Y. Zhang, G. Yuan and J. Li, *Jpn. J. Appl. Phys.*, 2016, **55**, 085501.
36 K. Kusaka, D. Taniguchi, T. Hanabusa and K. Tominaga, *Vacuum*, 2002, **66**, 441–446.
37 T. Aubert, M. B. Assouar, O. Legrani, O. Elmazria, C. Tiusan and S. Robert, *J. Vac. Sci. Technol., A*, 2011, **29**, 021010.
38 H. Y. Liu, G. S. Tang, F. Zeng and F. Pan, *J. Cryst. Growth*, 2013, **363**, 80–85.
39 J. Yu, Z. Hao, J. Wang, J. Deng, W. Yu, L. Wang, Y. Luo, Y. Han, C. Sun, B. Xiong and H. Li, *J. Alloys Compd.*, 2019, **783**, 633–642.
40 C. Ramesh, P. Tyagi, S. Bera, S. Gautam, K. M. Subhedar, M. S. Kumar and S. S. Kushvaha, *J. Nanosci. Nanotechnol.*, 2020, **20**, 3929–3934.
41 K. Chung, S. I. Park, H. Baek, J. S. Chung and G. C. Yi, *NPG Asia Mater.*, 2012, **4**, 1–5.
42 J. Kim, C. Bayram, H. Park, C. W. Cheng, C. Dimitrakopoulos, J. A. Ott, K. B. Reuter, S. W. Bedell and D. K. Sadana, *Nat. Commun.*, 2014, **5**, 1–7.
43 Y. Zhang, K. Su, R. Guo, S. Xu, D. Chen, J. Zhu, W. Bao, J. Zhang, J. Ning and Y. Hao, *Phys. Status Solidi RRL*, 2019, **13**, 1900167.
44 V. M. Kaganer, O. Brandt, A. Trampert and K. H. Ploog, *Phys. Rev. B: Condens. Matter Mater. Phys.*, 2008, **72**, 045423.
45 G. Li, Y. Y. Zhang, H. Guo, L. Huang, H. Lu, X. Lin, Y. L. Wang, S. Du and H. J. Gao, *Chem. Soc. Rev.*, 2018, **47**, 6073–6100.
46 Y. Qi, Y. Wang, Z. Pang, Z. Dou, T. Wei, P. Gao, S. Zhang, X. Xu, Z. Chang, B. Deng, S. Chen, Z. Chen, H. Ci, R. Wang, F. Zhao, J. Yan, X. Yi, K. Liu, H. Peng, Z. Liu, L. Tong, J. Zhang, Y. Wei, J. Li and Z. Liu, *J. Am. Chem. Soc.*, 2018, **140**, 11935–11941.
47 Y. Li, Y. Zhao, T. Wei, Z. Liu, R. Duan, Y. Wang, Z. Xiang, Q. Wu, J. Yan, X. Yi, G. Yuan, W. Junxi and J. Li, Jpn, *J. Appl. Phys.*, 2017, **56**, 085506.
48 W. C. Ke, Z. Y. Liang, S. T. Tesfay, C. Y. Chiang, C. Y. Yang, K. J. Chang and J. C. Lin, *Appl. Surf. Sci.*, 2019, **494**, 644–650.
49 Y. Kim, S. S. Cruz, K. Lee, B. O. Alawode, C. Choi, Y. Song, J. M. Johnson, C. Heidelberger, W. Kong, S. Choi, K. Qiao, I. Almansouri, E. A. Fitzgerald, J. Kong, A. M. Kolpak, J. Hwang and J. Kim, *Nature*, 2017, **544**, 340–343.
50 B. H. Hwang, C. S. Chen, H. Y. Lu and T. C. Hsu, *Mater. Sci. Eng., A*, 2002, **5**, 380–388.
51 K. P. Sharma, S. M. Shinde, M. S. Rosmi, S. Sharma, G. Kalita and M. Tanemura, *J. Mater. Sci.*, 2016, **51**, 7220–7228.